# Co-designed millimeter-wave and sub-6GHz antenna for 5G smartphones

Liang, Qiuyan; Aliakbari Abar, Hanieh; Lau, Buon Kiong

*Published in:*
IEEE Antennas and Wireless Propagation Letters

*DOI:*
10.1109/LAWP.2022.3187782

2022

*Document Version:*
Peer reviewed version (aka post-print)

# Co-designed Millimeter-wave and Sub-6GHz Antenna for 5G Smartphones

Qiuyan Liang, Hanieh Aliakbari, and Buon Kiong Lau, *Fellow, IEEE*

***Abstract*—This letter proposes a co-designed millimeter-wave (mm-wave) and sub-6GHz antenna system. The antenna system consists of four 28GHz mm-wave arrays with reconfigurable radiation patterns and two sub-6GHz antennas fed with two corner capacitive coupling elements (CCEs). Each corner CCE is formed by the connected ground planes of two mm-wave arrays in the shared-aperture configuration. The two CCEs are separately matched to cover two sub-6GHz bands. Each mm-wave array consists of an active patch element and two parasitic patch elements loaded with PIN diodes, realizing 90-degree beam scanning range with two states of the PIN diodes. The measured results of the fabricated prototype show good agreement with the simulated ones. The prototyped mm-wave arrays cover the band 27.5-28.35GHz, and each achieves 90-degree beam scanning at 28GHz, with measured peak realized gain of 7.9 dBi. The CCE ports cover the two sub-6GHz bands of 0.79-0.96 GHz and 1.7-5GHz, with measured isolation of above 17dB and 20dB, respectively. The mm-wave band isolation is above 26dB.**

***Index Terms*—co-designed antennas, terminal antennas, millimeter-wave antennas, reconfigurable antennas.**

## I. Introduction

With the widespread adoption of smartphones and the increasing use of bandwidth-hungry apps, there is demand for ever higher data rates in cellular communications. Millimeter wave (mm-wave) technology can facilitate higher data rates, due to more bandwidth being available at higher frequencies [1], [2]. But to compensate for high path loss in mm-wave bands to ensure sufficient coverage area, mm-wave antennas need to form steerable beams with high gains.

One popular approach for mm-wave beam-steering is to use conventional phased array antennas [3]-[7]. However, phase shifters can incur considerable insertion loss and phased array elements can occupy a relatively large volume in a smartphone [8]. To facilitate a compact radiator and avoid the use of phase shifters, a 28GHz array with parasitic elements is proposed [8]. The beam-steering is realized by shorting the parasitic elements via four transmission lines of different lengths. However, no real switch is used in the measurement and the transmission lines occupy considerable PCB space.

To fit multiple antennas working in widely separated bands into the limited space of a smartphone, co-design of the mm-wave antenna and sub-6GHz antenna has been studied [9]-[17]. In [9] and [10], the mm-wave arrays with feeding networks and the sub-6GHz antennas (chip antennas/ monopoles) are designed in separate spaces and they do not affect each other. In [11] and [12], the slot structure acting as a mm-wave connected array is cleverly reused as a defected ground structure to improves the isolation between the sub-6GHz antennas. However, the array and sub-6GHz antennas still occupy separate spaces.

To improve aperture utilization, a frequency-reconfigurable slot antenna with a varactor diode working in a 4G band is reused as a mm-wave antenna based on the connected slot array concept [13]. However, its 4G band is limited to 2.05-2.7GHz. As another share-aperture approach, the mm-wave array module is embedded into the metal bezel present in some smartphones, with the bezel serving as the sub-6GHz antenna [14]-[16]. This method helps to reduce the blockage of the mm-wave antenna radiation due to the metallic frame. Similarly, the addition of grating strips facilitates the reuse of the PCB space occupied by a low-band planar inverted-F antenna (PIFA) for implementing a mm-wave antenna array [17]. However, the mm-wave antennas in [14]-[17] are still phased arrays with lossy feeding networks, and some sub-6GHz antennas (e.g., PIFA) occupy relatively large spaces.

In this work, a co-designed smartphone antenna system is proposed to accommodate four mm-wave arrays and two sub-6GHz antennas in a compact space. The mm-wave array employs parasitic elements loaded with PIN diodes to achieve beam-steering, in the same manner as Yagi-Uda antenna [18]. Instead of using self-resonant elements, the sub-6GHz antennas are excited by non-resonant capacitive coupling elements (CCEs) [19], which are becoming popular to realize low cellular band antennas due to their compactness and simple structure (see [20] and references therein). The metal ground planes of the mm-wave arrays are shared by the corner CCEs that excite the sub-6GHz bands. This shared-aperture configuration with compact mm-wave arrays on the corner CCEs facilitates sleek integration into 5G smartphones. The fabricated prototype confirms that each mm-wave array can realize 90° scanning range with good impedance matching in the desired frequency band of 27.5-28.35GHz. Therefore, the four mm-wave arrays on the two CCEs enable full 360° coverage. The two sub-6GHz antennas are well matched in the operating bands of 0.79-0.96GHz and 1.7-5GHz, respectively.

## II. Co-designed Antenna System

Figure 1 provides the 3D view and top view of the proposed co-designed antenna system. It consists of four mm-wave arrays mounted on two corner CCEs and a 120mm × 60mm chassis excited by the two CCEs to cover two sub-6GHz bands. The proposed antenna system is further described below.

Manuscript received Jan. 8, 2022, revised May 8, 2022. This work was supported in part by Vetenskapsrådet under Grant No. 2018-04717

Qiuyan Liang is with Department of Electrical and Information Technology, Lund University, Lund 22363, Sweden, and also with National Key Laboratory of Antenna and Microwave Technology, Xidian University, Xi'an 710071, China. (e-mail: qiuyan.liang@eit.lth.se)

Hanieh Aliakbari and Buon Kiong Lau are with Department of Electrical and Information Technology, Lund University, Lund 22363, Sweden.

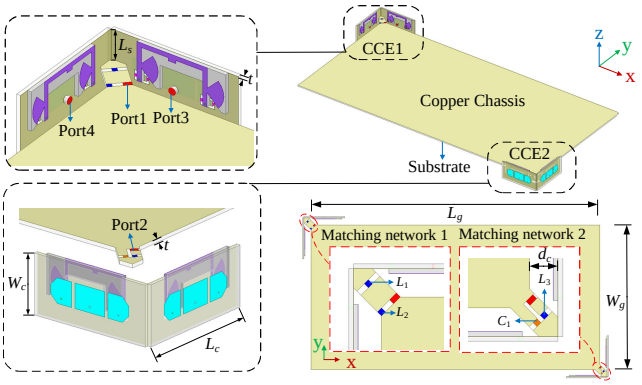


Fig. 1. Overall structure of proposed co-designed antenna ($L_s$ = 4mm, $L_c$ = 17mm, $W_c$ = 8mm, $t$ = 0.508mm, $L_g$ = 120mm, $W_g$ = 60mm, $d_c$ = 3mm).

### A. *Mm-wave Antenna Array*

As shown in Fig. 2, the antenna array uses two layers of substrate (Rogers 5880, with thickness of 0.508mm, relative permittivity of 2.2 and loss tangent of 0.0009) for the radiating layer (Sub1) and the direct current (DC) control layer (Sub2). The array is composed of an active element fed with a 50Ω coaxial cable and two passive elements symmetrically located on two sides of the active element. Each passive element is loaded with two PIN diodes bonded over a square slot etched on the ground. The DC biasing lines are printed on the bottom layer of Sub2. Two shorting pins connect the DC biasing lines, the passive elements and the metal sheets within the etched slots. The two sets of PIN diodes for the two passive elements are installed with opposite bias directions and their DC biasing lines with isolation fan stubs are connected in parallel to share a DC feeding pad. The opposite bias ensures that, when a DC voltage is applied, the PIN diodes of one passive element will always be in the opposite state to those of the other passive element (i.e., ON and OFF states for passive elements 1 and 2, respectively, or vice-versa). The PIN diodes, produced by MACOM (Model no. MA4GP907), allow for operation up to millimeter frequencies [21]. Its equivalent circuits for the ON and OFF states in mm-wave bands, as shown in Fig. 3, were used in the simulation model, where the insertion loss of the PIN diode in the ON and OFF state is modeled with a 5.2Ω and a 10kΩ resistor, respectively.

The parasitic element is connected to/disconnected from the ground plane when the beneath PIN diodes are turned ON/OFF, which decreases/increases its effective electrical size, such that it acts as a director/reflector [22]. The beam of this array is steered to the director and away from the reflector based on the principle of Yagi-Uda antenna. By applying positive or negative DC voltage between the DC biasing pad and the ground, two symmetrical beams can be achieved.

The effects of the structural parameters were investigated using ANSYS HFSS 2021. The simulation results show that the beam deflection angle and sidelobe level (SLL) are mainly dependent on the size of the parasitic elements (controlled by $a$) and the distance between the parasitic elements and the active one ($d$) (see Fig. 2(b)). For example, decreasing $a$ or increasing $d$ will lead to increased beam deflection angle and SLL, as well as narrower main beam. The appropriate $a$ and $d$ values were then optimized to obtain ±45° beam deflection (i.e., mirror symmetric beams for the two possible states of the diodes) and low SLL. The impedance bandwidth of the antenna becomes wider when $d$ decreases, which is because of that a second (higher) resonance is introduced by the parasitic element in the ON state. Considering the radiation pattern performance and the fabrication tolerance requirements, the distance $d$ = 0.5mm was finally chosen.

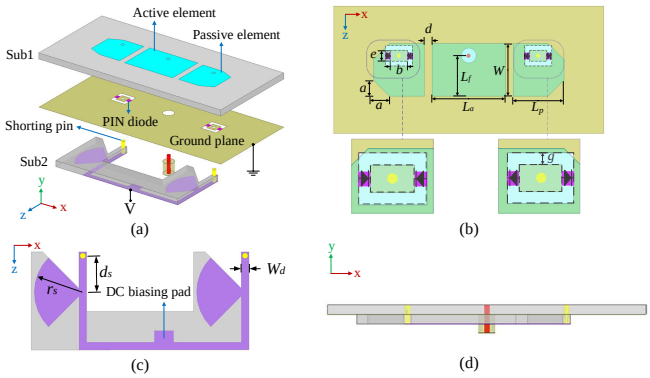


Fig. 2. Geometry of mm-wave array fed by Port3: (a) 3D exploded view, (b) top view ($a$ = 1mm, $b$ = 1.1mm, $d$ = 0.5mm, $e$ = 0.7mm, $L_a$ = 4.6mm, $L_f$ = 2.6mm, $L_p$ = 3.2mm, $W$ = 3.3mm, $g$ = 0.3mm), (c) DC biasing lines ($r_s$ = 1.8mm, $d_s$ = 2.2mm, $W_d$ = 0.6mm), (d) side view.

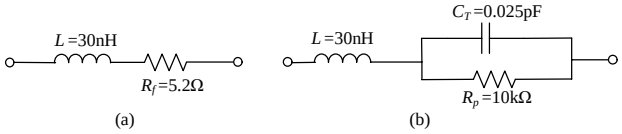


Fig. 3. Equivalent circuits of PIN diode in (a) ON state and (b) OFF state.

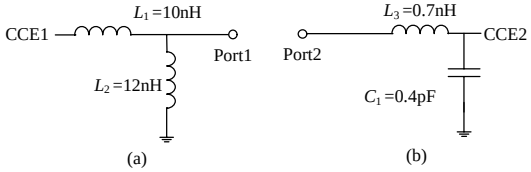


Fig. 4. Schematics of matching networks for (a) CCE1 and (b) CCE2.


Fig. 5. Proposed antenna system with metal frame.

### B. *Sub-6GHz antennas*

Since the CCE should be placed in the region of maximum electric field maximum strength of the mode to be excited (i.e., the fundamental dipole mode) [23], two CCEs are placed at two diagonally opposite corners of the chassis. In addition, these cirner locations enable the four mm-wave antennas on the two CCEs to cover the entire field of view and mitigate blockage from the user's hand(s). CCE1 and CCE2 excite the chassis through matching networks (see Figs. 1 and 4) designed in Betamatch [24] to realize two sub-6GHz antennas, i.e., Port1 and Port2 cover the low band (LB) of 0.79-0.96GHz and the high band (HB) of 1.71-5GHz, respectively. Larger CCE size facilitates broader bandwidth of Port1, thus the CCE parameters is chosen considering the trade-off between the bandwidth and size [25]. The bandwidth of Port1 and the isolation between Port1 and Port2 in the LB mainly depend on

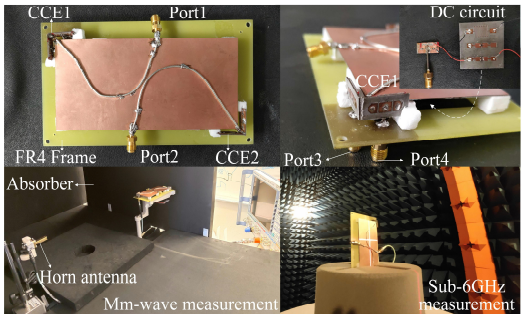


Fig. 6. Prototype of proposed antenna system and measurement setups.

the inductance $L_1$. With decreasing $L_1$, the LB bandwidth increases whereas the Port1-Port2 isolation decreases. To achieve a good trade-off between bandwidth and isolation, the matching elements in matching network 1 were chosen to be $L_1$ = 10nH and $L_2$ = 12nH. The bandwidth of Port2 in the HB mainly depends on the capacitance value $C_1$. The Port1-Port2 isolation in HB is not significantly affected by the matching elements. The optimized matching elements in matching network 2 are $C_1$ = 0.4pF and $L_3$ = 0.7nH. It is noted that the loading effect of the mm-wave connectors has been included in the design of matching networks, to facilitate experimental validation. In practice, these connectors are not needed and the matching network can be updated by changing the matching circuit parameter values (e.g., $L_1$ = 18nH and $L_2$ = 10nH for port 1). Moreover, more matching elements can give a larger Port2 bandwidth (e.g., 1.37-6.71GHz using five elements) [24].

In practical applications, smartphones are equipped with a touch screen and some come with metal bezels (side frames). It is found that adding a metal plate (of the same size as the chassis) 4mm above the chassis (and grounded through a shorting pin at the chassis center) to model the screen does not affect the fundamental dipole mode of the chassis [26], and the impedance matching in the sub-6GHz bands can be restored by updating the matching networks. To study the effect of metal bezels, four separate vertical metal strips of 8mm width were located along (but not connected to) the four sides of the chassis, as depicted in Fig. 5. When the distance $d_1$ between the strips and the CCE1 is larger than 5mm (0.015 wavelength in free space at 0.875GHz), Port1 retains over 90% of the original bandwidth (i.e., the case with no strip). The distance $d_2$ for the CCE2 to retain at least 90% of the original bandwidth is 2mm (0.023 wavelength in free space at 3.5GHz).

## III. Simulated and Measured Results

A prototype of the smartphone antenna system was fabricated (see Fig. 6). The mm-wave CAB.058 coaxial cables are used to feed the mm-wave arrays on CCE1 in the measurement, which are intended to verify the beam scanning range of the mm-wave arrays on each CCE. In real implementation, the feeding of the mm-wave antenna should be realized with more advanced integrated technology to minimize any possible interference. The DC voltage is applied through a substrate with the DC circuits, which is attached on the back side of the chassis. An FR4 frame is designed to support the antennas in the measurement.

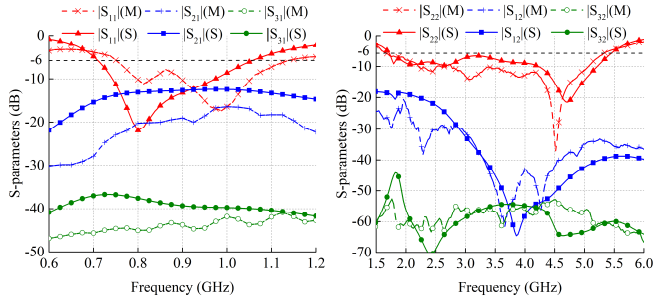


Fig. 7. Simulated (S) and measured (M) S-parameters of sub-6GHz antennas.

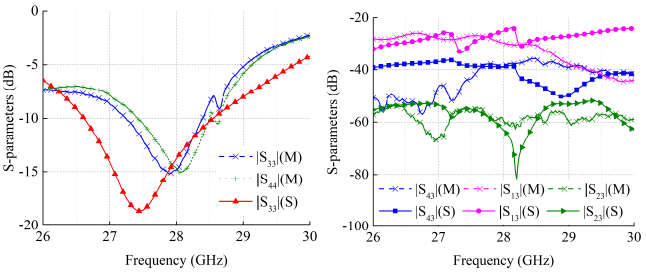


Fig. 8. Simulated (S) and measured (M) S-parameters of mm-wave array.

### A. S-Parameters

Fig. 7 shows the S-parameter results of the two sub-6GHz antennas. The measured 6dB impedance bandwidth (VSWR of 3:1) of Port1 is 0.38GHz (0.75-1.13GHz), covering the LTE800/850/900 bands. In the operating band (i.e., LB), the measured isolation of the sub-6GHz ports $|S_{21}|$ is larger than 17dB and that between Port1 and mm-wave port Port3 $|S_{31}|$ is larger than 43dB. The measured 6dB impedance bandwidth of Port2 is 3.6GHz (1.70-5.30GHz), covering the LTE1700-2600 and 5G NR n77-79 bands. In this upper band (i.e., HB), the measured isolations with other ports are over 20dB.

The S-parameter results of the mm-wave array are shown in Fig. 8. Port3 and Port4 have the same simulation results for reflection coefficient due to symmetry. The simulated 10dB bandwidth of the mm-wave antenna is around 2GHz (26.56-28.54GHz). It is noted that, if needed, the mm-wave antenna bandwidth can be significantly enhanced (e.g., to 3GHz) by using a stacked patch as the active element. The measured resonances are slightly higher than those in simulation and the measured bandwidths are narrower than the simulated ones, due to the tolerance in the soldering of the mm-wave cables. Such discrepancy is common in mm-wave bands due to the relatively small wavelengths [13]-[17]. The measured 10dB bandwidths of Port3 and Port4 are 1.15GHz (27.25-28.4GHz) a 1.1GHz (27.4-28.5GHz), respectively, covering the 5G NR n261 band. In the operating mm-wave band, the measured isolations with other ports are over 26dB.

### B. Radiation Patterns

The radiation pattern results of the fabricated prototype in the sub-6GHz bands were obtained from a SATIMO multi-probe spherical near-field system [27]. Figure 9 shows the normalized simulated and measured 2-D pattern cuts at $\theta$ = 90° (azimuth cut), $\varphi$ = 0° (elevation cut), and $\varphi$ = 90° (elevation cut) for Port1 and Port2 at 0.875 GHz in LB and 3.5 GHz in HB, respectively. The fundamental dipole mode of the chassis is excited by the CCEs in the two sub-6GHz antennas.

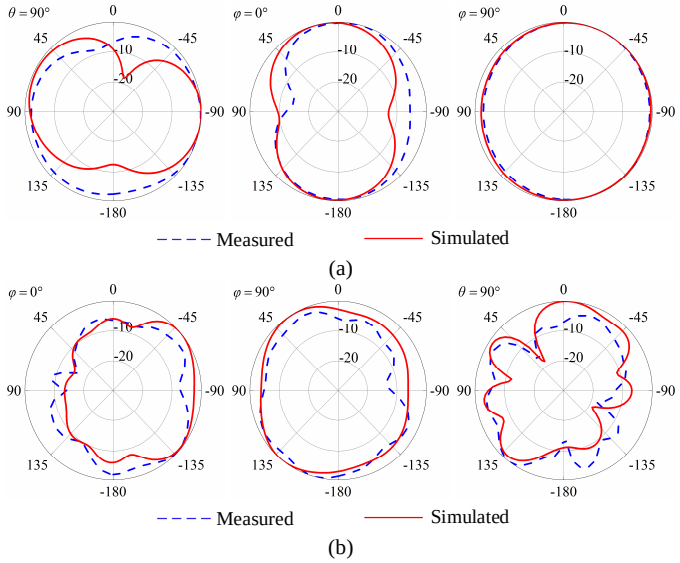


Fig. 9. Simulated and measured normalized radiation patterns at sub-6GHz band in (a) LB (0.875 GHz) and (b) HB (3.5GHz).

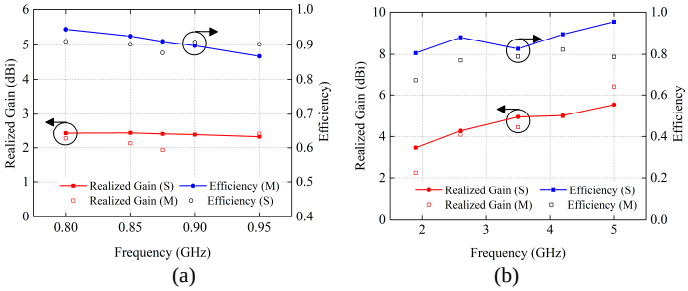


Fig. 10. Simulated (S) and measured (M) realized gain and efficiency in sub-6GHz in (a) LB and (b) HB.

The discrepancies between the simulated and measured patterns are primarily due to the presence of a feed cable in the near field of the structure. The simulated and measured realized gain and efficiency in the sub-6GHz bands are shown in Fig. 10. The measured efficiencies are higher than the simulated ones at some frequency points due to the discrepancies between the measured and simulated S-parameters.

Figure 11 shows the radiation patterns of two mm-wave arrays on CCE1 at 28GHz, which were measured with an in-house pattern measurement system utilizing the Rohde and Schwarz vector network analyzer ZVA67. Applying the positive/negative voltages on the DC biasing pads of the two mm-wave arrays, four deflected beams were realized. The two mm-wave arrays on CCE1 can achieve 180° coverage range with half power beamwidth. The peak measured realized gains are 7.4dBi or 7.9dBi (Port3 with positive or negative voltage) and 7.1dBi or 7.7dBi (Port4 positive or negative voltage). The peak measured realized gains are less than the simulated ones by 1.4dBi (Port3 positive), 1.2dBi (Port3 negative), 1.6dBi (Port4 positive) and 1.3dBi (Port4 negative), respectively. The realized gain difference is primarily due to the loss in the mm-wave cables and slight pattern shape discrepancy, the latter of which was caused by inaccuracies in the PIN diode's equivalent circuits and the tolerance of the measurement system.

### *C. Comparison with Other Sub-6GHz/Mm-Wave Antennas*

A comparison of recent co-designed antennas for sub-6GHz and mm-wave bands is presented in Table I. The sub-6GHz antennas in [14] and [17] employ self-resonance structures, which occupy larger volumes. Phased arrays, which require feeding networks, are used for the mm-wave antennas in [13], [14] and [17]. The proposed antenna system can cover wider sub-6GHz bands despite the use of two compact CCEs. With the parasitic elements, the proposed mm-wave array achieves beam scanning without the need for complex feeding networks. Moreover, the shared-aperture configuration of the corner CCEs and mm-wave arrays enables a compact antenna volume.

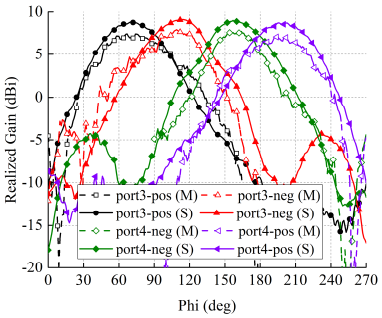


Fig. 11. Simulated (S) and measured (M) radiation patterns of mm-wave arrays with positive (pos) and negative (neg) voltage at 28 GHz.

TABLE I
COMPARISON BETWEEN THE PROPOSED AND PREVIOUS 4G/5G DESIGNS

| | Frequency range (GHz) | Total antenna volume ($mm^3$) | Phased array (mm-wave) | Diodes |
|---|---|---|---|---|
| [13] | 2.05-2.7 and 23-29 | 35×12.28×0.381 | yes | yes |
| [14] | 0.7-0.96, 1.71-2.69 and 25-30 | 75×10×7 | yes | no |
| [16] | 0.76-0.98, 1.24-2.87, and 22-28.4 | 21.7×7.75×0.64 | Active and dummy elements | no |
| [17] | 0.74-0.96, 1.7-2.2, and 22-31 | 70×9×0.764 | yes | no |
| This work | 0.75-1.13, 1.7-5.3 and 27.5-28.35 | 34×8×1.016×2 | no | yes |

## IV. CONCLUSION

A co-designed mm-wave and sub-6GHz antenna system for 5G smartphone application is proposed in this letter. Each mm-wave array antenna uses two parasitic elements loaded with PIN diodes to realize beam scanning. The four mm-wave arrays share the aperture of the CCEs, with the latter providing coverage of two sub-6GHz bands, which facilitates a compact antenna structure. The measured results show that the sub-6GHz antennas cover the bands of 0.79-0.96 GHz and 1.71-5 GHz. The mm-wave array provides 90° scanning range with measured realized gain of up to 7.9dBi at 28GHz. Possible future work includes adding ports in the sub-6GHz bands for MIMO operation by means of creating and exciting more resonant modes [20] as well as using more parasitic elements and reconfigurable states for higher gain in mm-wave bands.

## ACKNOWLEDGEMENT

The authors would like to thank A. Johansson of Lund University and D. Pugachev of Sigma Connectivity for their help in prototype fabrication and pattern measurement.

## REFERENCES


[1] T. S. Rappaport, *et al*., "Millimeter wave mobile communications for 5G cellular: It will work!" *IEEE Access*, vol. 1, pp. 335-349, 2013.

[2] W. Hong, K.-H. Baek, and S. Ko, "Millimeter-wave 5G antennas for smartphones: Overview and experimental demonstration," *IEEE Trans. Antennas Propag*., vol. 65, no. 12, pp. 6250-6261, Dec. 2017.

[3] N. Ojaroudiparchin, M. Shen, S. Zhang, and G. F. Pedersen, "A switchable 3-D-coverage-phased array antenna package for 5G mobile terminals," *IEEE Antennas Wireless Propag. Lett.*, vol. 15, pp. 1747-1750, Feb. 2016.

[4] S. Zhang, X. Chen, I. Syrytsin, and G. F. Pedersen, "A planar switchable 3-D-coverage phased array antenna and its user effects for 28-GHz mobile terminal applications," *IEEE Trans. Antennas Propag*., vol. 65, no. 12, pp. 6413-6421, Dec. 2017.

[5] I. Syrytsin, S. Zhang, G. F. Pedersen, and A. S. Morris, "Compact quad-mode planar phased array with wideband for 5G mobile terminals," *IEEE Trans. Antennas Propag*., vol. 66, no. 9, pp. 4648-4657, Sep. 2018.

[6] W. Hong, K. Baek, Youngju Lee, and Yoon Geon Kim, "Design and analysis of a low-profile 28 GHz beam steering antenna solution for Future 5G cellular applications," in *Proc. IEEE MTT-S Int. Microw. Symp. (IMS)*, Tampa, USA, Jun. 1-6, 2014, pp. 1-4.

[7] N. Ojaroudiparchin, M. Shen, and G. F. Pedersen, "A 28 GHz FR-4 compatible phased array antenna for 5G mobile phone applications," in *Proc. Int. Symp. Antennas Propag. (ISAP)*, Hobart, Australia, Nov. 9-12, 2015, pp. 1-4.

[8] S. Zhang, I. Syrytsin, and G. F. Pedersen, "Compact beam-steerable antenna array with two passive parasitic elements for 5G mobile terminals at 28 GHz," *IEEE Trans. Antennas Propag*., vol. 66, no. 10, pp. 5193-5203, Oct. 2018.

[9] C. Lee, M. K. Khattak, and S. Kahng, "Wideband 5G beamforming printed array clutched by LTE-A $4 \times 4$-multiple-input–multiple-output antennas with high isolation," *IET Microw. Antennas Propag*., vol. 12, no. 8, pp. 1407-1413, Mar. 2018.

[10] R. Hussain, A. T. Alreshaid, S. K. Podilchak, and M. S. Sharawi, "Compact 4G MIMO antenna integrated with a 5G array for current and future mobile handsets," *IET Microw. Antennas Propag*., vol. 11, no. 2, pp. 271-279, Jan. 2017.

[11] M. Ikram, R. Hussain, and M. S. Sharawi, "4G/5G antenna system with dual function planar connected array," *IET Microw. Antennas Propag*., vol. 11, no. 12, pp. 1760-1764, Sep. 2017.

[12] M. S. Sharawi, M. Ikram, and A. Shamim, "A two concentric slot loop based connected array MIMO antenna system for 4G/5G terminals," *IEEE Trans. Antennas Propag*., vol. 65, no. 12, pp. 6679-6686, Dec. 2017.

[13] M. Ikram, E. A. Abbas, N. Nguyen-Trong, K. H. Sayidmarie, and A. Abbosh, "Integrated frequency-reconfigurable slot antenna and connected slot antenna array for 4G and 5G mobile handsets," *IEEE Trans. Antennas Propag*., vol. 67, no. 12, pp. 7225-7233, Dec. 2019.

[14] J. Kurvinen, H. Kähkönen, A. Lehtovuori, J. Ala-Laurinaho, and V. Viikari, "Co-designed mm-Wave and LTE handset antennas," *IEEE Trans. Antennas Propag*., vol. 67, no. 3, pp. 1545-1553, Mar. 2019.

[15] R. Montoya Moreno, J. Ala-Laurinaho, A. Khripkov, J. Ilvonen, and V. Viikari, "Dual-polarized mm-wave endfire antenna for mobile devices," *IEEE Trans. Antennas Propag*., vol. 68, no. 8, pp. 5924-5934, Aug. 2020.

[16] R. Rodriguez-Cano, S. Zhang, K. Zhao, and G. F. Pedersen, "Mm-wave beam-steerable endfire array embedded in a slotted metal-frame LTE antenna," *IEEE Trans. Antennas Propag*., vol. 68, no. 5, pp. 3685-3694, May 2020.

[17] M. M. Samadi Taheri, A. Abdipour, S. Zhang, and G. F. Pedersen, "Integrated millimeter-wave wideband end-fire 5G beam steerable array and low-frequency 4G LTE antenna in mobile terminals," *IEEE Trans. Veh. Technol.*, vol. 68, no. 4, pp. 4042-4046, Apr. 2019.

[18] J. Huang and A. C. Densmore, "Microstrip Yagi array antenna for mobile satellite vehicle application," *IEEE Trans. Antennas Propag.*, vol. 39, no. 7, pp. 1024-1030, Jul. 1991.

[19] J. Villanen, J. Ollikainen, O. Kivekas, and P. Vainikainen, "Coupling element based mobile terminal antenna structures," *IEEE Trans. Antennas Propag*., vol. 54, no. 7, pp. 2142-2153, Jul. 2006.

[20] H. Aliakbari, and B. K. Lau, "Low-profile two-port MIMO terminal antenna for low LTE bands with wideband multimodal excitation," *IEEE Open J. Antennas Propag*., vol. 1, pp. 368-378, 2020.

[21] MACOM. (2016). *Products: MA4GP907*. [Online]. Available: http://cdn.macom.com/datasheets/MA4GP907.pdf

[22] W. Deng, X. Yang, C. Shen, J. Zhao, and B. Wang, "A dual-polarized pattern reconfigurable Yagi patch antenna for microbase stations," *IEEE Trans. Antennas Propag*., vol. 65, no. 10, pp. 5095-5102, Oct. 2017.

[23] R. Valkonen, M. Kaltiokallio, and C. Icheln, "Capacitive coupling element antennas for multi-standard mobile handsets," *IEEE Trans. on Antennas Propag*., vol. 61, no. 5, pp. 2783-2791, May 2013.

[24] Betamatch. (2019). *MNW Scan Pte Ltd, Version 3.7.6*. Accessed: Nov. 11, 2021. [Online]. Available: http://www.mnw-scan.com

[25] H. Aliakbari, and B. K. Lau, "Impact of capacitive coupling element design on antenna bandwidth," in *Proc. 12th Europ. Conf. Antennas Propag. (EuCAP)*, London, UK, Apr. 9-13, 2018, pp. 1-4.

[26] H. Aliakbari, L. Y. Nie and B. K. Lau, "Large screen enabled tri-Port MIMO handset antenna for low LTE bands," *IEEE Open Journal of Antennas and Propag*., vol. 2, pp. 911-920, Aug. 2021.

[27] Satimo Stargate. (2019). *Measurement System*. Accessed: Aug. 26, 2021. [Online]. Available: http://www.satimo.com